

Microwave plasma CVD growth and characterization of polycrystalline diamond films on β -Ga₂O₃

Saleh Ahmed Khan¹, Stephen Margiotta¹, Ahmed Ibreljic¹, Anhar Bhuiyan^{1, a)}

¹*Department of Electrical and Computer Engineering, University of Massachusetts Lowell, MA 01854, USA*

^{a)} Corresponding author Email: anhar_bhuiyan@uml.edu

Abstract

The integration of diamond with β -Ga₂O₃ presents a promising pathway to enhance thermal management in high-power electronic devices, where the inherently low thermal conductivity of β -Ga₂O₃ can lead to localized self-heating and elevated junction temperatures. In this work, we demonstrate a scalable, low-damage approach to integrate polycrystalline diamond films on (010) β -Ga₂O₃ substrates via microwave plasma chemical vapor deposition (MPCVD), employing dielectric interlayers and polymer-assisted electrostatic nanodiamond seeding to systematically evaluate the impact of growth conditions on film morphology, grain evolution, phase purity, and optical characteristics. At the growth temperature of 800 °C, progressive grain coarsening is observed with extended deposition, with lateral grain size increasing from 37.6 nm (53 nm thickness) to 192.5 nm for an 886 nm film. This microstructural evolution is accompanied by narrowing of the diamond Raman peak and a monotonic increase in sp³-phase fraction from 95.9% to as high as 98.9%, indicating continued suppression of non-diamond carbon with prolonged growth. Comparison of SiO₂ and SiN_x interlayers under identical growth conditions shows only marginal differences in grain size and phase purity, indicating limited interlayer influence once high nucleation density is established. Importantly, diamond films exhibiting >96% sp³-phase content were achieved at substrate temperatures as low as 480 °C, highlighting the viability of diamond-on-Ga₂O₃ integration under reduced thermal budgets. These findings establish a robust,

This is the author's peer reviewed, accepted manuscript. However, the online version of record will be different from this version once it has been copyedited and typeset.

PLEASE CITE THIS ARTICLE AS DOI: 10.1063/1.50333162

scalable platform for integrating diamond on β -Ga₂O₃, supporting the development of next-generation power and RF devices with improved thermal management.

Keywords: *Ultra-wide bandgap semiconductor, polycrystalline Diamond, β -Ga₂O₃, thermal management, microwave plasma CVD*

The ultrawide bandgap β -Ga₂O₃ has emerged as a promising semiconductor for next-generation power electronics, owing to its large bandgap (~4.8 eV), high critical electric field (~8 MV/cm), and the availability of low-cost, melt-grown large area native substrates [1-4]. However, a critical limitation hindering the widespread adoption of Ga₂O₃ in high-power applications is its intrinsically low thermal conductivity (10-27 W/m·K) [5]. This poor heat dissipation capability leads to severe thermal management challenges under high power densities, resulting in localized hot spots, device degradation, and long-term reliability concerns [6,7].

An effective approach to overcoming thermal limitations in β -Ga₂O₃ devices involves integrating materials with superior thermal conductivity. Diamond, in particular, offers a compelling solution due to its exceptional thermal conductivity, surpassing 2000 W/m·K in single-crystal form [8] and reaching 1000-1800 W/m·K in optimized polycrystalline films [9], along with its wide bandgap, outstanding mechanical strength, and chemical stability [10-13]. Prior efforts involving GaN-on-diamond integration have demonstrated substantial reductions in thermal resistance and junction temperature through the use of microwave plasma-enhanced chemical vapor deposition (MPCVD)-grown polycrystalline diamond layers. These advances were enabled by careful interface engineering to promote nucleation and protect the underlying device structure during growth [14-23]. Various seeding strategies have also been developed to address the challenge of initiating diamond nucleation on non-diamond surfaces, including mechanical abrasion [24-27], bias-enhanced nucleation [28, 29], chemical nucleation using adamantane

This is the author's peer reviewed, accepted manuscript. However, the online version of record will be different from this version once it has been copyedited and typeset.

PLEASE CITE THIS ARTICLE AS DOI: 10.1063/5.0333162

derivatives [30-33], and polymer-assisted electrostatic methods [34-36]. These approaches have achieved nucleation densities up to $\sim 10^{11} \text{ cm}^{-2}$ [37-38] and enabled coalesced films on foreign substrates.

However, translating this success to $\beta\text{-Ga}_2\text{O}_3$ has proven non-trivial. The surface energy mismatch between diamond ($\sim 6 \text{ J/m}^2$) and $\beta\text{-Ga}_2\text{O}_3$ ($\sim 1 \text{ J/m}^2$) can suppress nucleation and hinder lateral growth, often leading to sparse, discontinuous films or isolated diamond clusters unless appropriate interface treatments are applied [39-41]. Although a few studies have demonstrated the feasibility of diamond growth on $\beta\text{-Ga}_2\text{O}_3$ using interlayers such as SiO_2 [42] or $\text{Al}_2\text{O}_3/\text{SiO}_2$ [39] in combination with nanodiamond seeding [39,42,43], these efforts have primarily emphasized early-stage nucleation behavior. Systematic studies that explore how downstream MPCVD growth conditions affect film morphology, structural ordering, phase composition and optical characteristics remain largely unexplored. A deeper understanding of these interdependencies is essential to guide process optimization, improve material quality, and enable reproducible integration of diamond layers on $\beta\text{-Ga}_2\text{O}_3$. In this work, we conduct a systematic study of polycrystalline diamond growth on $\beta\text{-Ga}_2\text{O}_3$ substrates using MPCVD, targeting the development of conformal diamond films suitable for monolithic integration. By employing dielectric interlayers, followed by polymer-assisted electrostatic seeding with nanodiamond particles, we explore how growth temperature, interfacial chemistry, and deposition time influence film morphology, grain size, surface roughness, phase composition, and optical response. This comprehensive approach offers new insight into how MPCVD process conditions influence the growth kinetics, microstructure, and quality of diamond films on Ga_2O_3 , providing a foundation for future development of thermal management solutions in high-power electronics.

This is the author's peer reviewed, accepted manuscript. However, the online version of record will be different from this version once it has been copyedited and typeset.

PLEASE CITE THIS ARTICLE AS DOI: 10.1063/5.0333162

The diamond films were deposited on (010) β -Ga₂O₃ substrates using MPCVD method. To facilitate heterogeneous nucleation of diamond and simultaneously mitigate plasma-induced damage at the Ga₂O₃-diamond interface, a dielectric buffer layer with a thickness of \sim 50 nm was deposited via plasma-enhanced chemical vapor deposition at 300 °C. Two types of dielectric materials, amorphous SiO₂ and SiN_x, were explored to evaluate their influence on seeding efficiency and film morphology. To ensure uniform and high-density nucleation of diamond, we employed a three-step polymer-assisted nanodiamond (ND) seeding process, leveraging electrostatic self-assembly principles [44]. Each dielectric-coated Ga₂O₃ sample was immersed for 10 minutes in an aqueous solution of poly-diallyldimethylammonium chloride (PDDAC), a high molecular weight cationic polymer that renders the surface positively charged through quaternary ammonium functional groups [21,45]. Following this, the sample was immersed in a suspension of ND particles with diameters ranging from 5-10 nm and zeta potentials exceeding \pm 50 mV. The PDDAC and ND dipping steps were repeated three times to form a trilayer structure, ensuring a dense and uniform coverage of nanodiamond particles across the substrate. Subsequent rinsing with DI water and nitrogen blow drying removed unbound particles. The positive surface potential imparted by PDDAC enhances electrostatic attraction with negatively charged nanodiamonds [44], facilitating high nucleation density and uniform diamond film coalescence during growth. Diamond film growth was performed in a Seki Technotron AX5010-INT MPCVD tool. A hydrogen-rich CH₄/H₂ (3/300) mixture containing 1% methane was used as the plasma chemistry, with a total chamber pressure of 50 Torr and a constant microwave power of 1000 W. The substrate temperature ranged from 480 to 800°C. Growth durations were tuned from 10-150 minutes. In addition to β -Ga₂O₃, control growth experiments were carried out on sapphire and Si substrates using the same polymer-assisted nanodiamond seeding protocol and comparable MPCVD

This is the author's peer reviewed, accepted manuscript. However, the online version of record will be different from this version once it has been copyedited and typeset.

PLEASE CITE THIS ARTICLE AS DOI: 10.1063/1.50333162

conditions. On sapphire, films up to ~824 nm thickness exhibit sp^3 -phase purity of ~98.5%, while on Si substrates, films up to ~814 nm thickness reach ~98.9% sp^3 -phase purity. The corresponding data are provided in Figures S1 and S2 of the Supplementary Material. Post-growth characterization was conducted to evaluate structural, morphological, and optical properties. Surface morphology, grain size, and film continuity were examined using JEOL JSM 7401F field-emission scanning electron microscope (FESEM) while Raman spectra were recorded with a Horiba LabRam Evolution Multiline Raman Spectrometer employing a 532 nm diode-pumped solid-state laser. Surface roughness and topography were analyzed by atomic force microscopy (AFM) using a Park XE-10, and optical absorption characteristics were obtained from room-temperature UV-Vis-NIR spectrophotometry by utilizing an Agilent Cary 60 UV/Vis spectrophotometer.

Figure 1 presents the evolution of surface morphology and roughness of diamond films deposited on SiO_2 -coated β - Ga_2O_3 at a fixed substrate temperature of 800 °C. Growth durations were varied from 10 to 150 minutes to investigate grain evolution and faceting behavior under low-methane and hydrogen-rich plasma conditions. FESEM images [Figures 1(a-d)] show a progressive transition from densely packed nanocrystals to increasingly faceted and coarsened grain structures with increasing deposition time and thickness. After 10 minutes [Figure 1(a)], the film is composed of densely packed, rounded grains with an average lateral grain size of 37.6 nm and film thickness of ~53 nm. Grain boundaries are not well defined, indicating early-stage vertical growth with limited lateral expansion. This morphology is consistent with high nucleation density achieved through multilayer polymer-assisted seeding using PDDAC and nanodiamond particles, which promotes rapid surface coverage and suppresses secondary nucleation [42]. At 30 minutes [Figure 1(b)], the grain size increases significantly to 91.0 nm, and faceting becomes more

This is the author's peer reviewed, accepted manuscript. However, the online version of record will be different from this version once it has been copyedited and typeset.

PLEASE CITE THIS ARTICLE AS DOI: 10.1063/1.50333162

pronounced, suggesting the onset of competitive grain growth. After 60 minutes of deposition [Figure 1(c)], the grain size further increases to 126.6 nm with well-defined grain boundaries and angular crystallites, indicating that lateral growth and facet sharpening dominate in the steady-state growth regime. The corresponding film thickness increases to 315 nm, confirming a vertical deposition rate of 5.25 nm/min. Upon extending the growth duration to 150 minutes [Figure 1(d)], the film thickness increases to 886 nm (growth rate of 5.91 nm/min), and the average lateral grain size further increases to 192.5 nm. The microstructure exhibits well-developed faceted grains with reduced grain boundary density, indicative of continued grain competition and coalescence. This progressive grain coarsening with thickness is consistent with thickness-dependent microstructural refinement during prolonged MPCVD growth and aligns with grain selection and competitive faceting behavior reported for low-CH₄ diamond growth on GaN and oxide-buffered substrates [18,21,42]. AFM topography scans, shown in Figures 1(e-h), quantitatively confirm the systematic increase in surface roughness associated with grain coarsening. The root mean square (RMS) roughness increases from 9.4 nm at 10 minutes to 13.2 nm at 30 minutes, reaching 16.3 nm at 60 minutes, and further increasing to 25.7 nm at 150 minutes. This monotonic increase reflects enhanced facet development and increased vertical height contrast between coalesced grains as the film thickens. Importantly, despite the substantial increase in thickness to nearly 900 nm, the film remains continuous, conformal, and free of delamination or pinholes, demonstrating robust adhesion to the underlying SiO₂ interlayer. The SiO₂ serves as a thermally stable and chemically inert diffusion barrier, while also providing a negatively charged surface conducive to electrostatic nanodiamond seed attachment [39,42].

Figure 2 shows the room-temperature Raman spectra of the diamond films grown on SiO₂/β-Ga₂O₃ substrates at 800 °C for deposition times ranging from 10 to 150 minutes. All spectra

This is the author's peer reviewed, accepted manuscript. However, the online version of record will be different from this version once it has been copyedited and typeset.

PLEASE CITE THIS ARTICLE AS DOI: 10.1063/1.50333162

display the first-order Raman peak associated with sp^3 -bonded diamond near 1332 cm^{-1} , confirming successful phase formation under hydrogen-rich MPCVD conditions. A systematic evolution of the diamond peak is observed with increasing growth duration and film thickness. The full width at half maximum (FWHM) decreases from 74.6 cm^{-1} for the 53 nm film to 65.5 cm^{-1} for the 157 nm film and 52.98 cm^{-1} for the 315 nm film, reaching 51.34 cm^{-1} for the 886 nm thick film. This progressive narrowing is consistent with the grain coarsening observed in FESEM and indicates improved structural order and reduced phonon confinement as the microstructure evolves [21,46]. In addition to peak sharpening, the relative intensity of the non-diamond carbon features decreases with continued growth. Secondary spectral features in the $1100\text{-}1600\text{ cm}^{-1}$ region include a shoulder near $\sim 1150\text{ cm}^{-1}$ attributed to trans-polyacetylene and a G-band centered around $\sim 1550\text{ cm}^{-1}$ associated with disordered sp^2 -bonded carbon [21,42,43]. While these features are more pronounced in thinner films, their relative contribution diminishes in thicker films, indicating progressive suppression of sp^2 -bonded carbon with extended deposition.

Figure 3 presents the evolution of key morphological and spectroscopic properties as a function of film thickness. Data points correspond to the four films characterized in Figures 1 and 2, with measured thicknesses of 53, 157, 315, and 886 nm for growth durations of 10, 30, 60, and 150 minutes, respectively. In Figure 3(a), both average grain size and surface roughness show a clear and systematic increase with increasing film thickness. These trends confirm that grain coarsening and surface topography evolve concurrently as the film develops. The continuous increase in grain size across the entire thickness range indicates sustained competitive grain growth and lateral expansion without significant secondary nucleation. Similar microstructural evolution has been reported in MPCVD-grown diamond, where continued deposition promotes coalescence of favorably oriented crystallites and reduction of grain boundary density [18]. Figure 3(b) shows

the corresponding evolution of Raman FWHM and sp^3 -phase purity. The FWHM of the diamond peak decreases from 74.6 cm^{-1} for the 53 nm film to 51.34 cm^{-1} for the 886 nm thick film. The phase purity of the diamond layer, expressed as the sp^3 -phase fraction, was estimated from integrated Raman peak area analysis [18,47-49]. In this method, the integrated area of the diamond peak near 1332 cm^{-1} is compared to the combined area of non-diamond carbon contributions, and a correction factor of 75 is applied to account for the higher Raman scattering efficiency of sp^2 -bonded carbon relative to sp^3 -bonded carbon [18,48,49]. Using this approach, the estimated sp^3 -phase purity increases monotonically from 95.9% (53 nm) to 96.7% (157 nm), then to 97.1% (315 nm), and ultimately reaches as high as 98.9% for the 886 nm film. This monotonic enhancement suggests effective suppression of sp^2 -bonded carbon during extended growth [18,50], as well as better-defined grain boundaries with reduced disorder.

Figure 4 compares the surface morphology and roughness of diamond films grown at three different substrate temperatures: 480 °C, 600 °C, and 800 °C. The growth durations were 120, 60, and 150 minutes, respectively, yielding thicknesses of 58.1 nm, 110.4 nm, and 886 nm. These correspond to growth rates of 29.1, 110.4, and 354.4 nm/hr, respectively. At 480 °C [Figures 4(a-b)], the film exhibits a compact but fine-grained morphology, with an average grain size of 46.8 nm and an RMS roughness of 10.4 nm. The relatively low growth rate and limited adatom mobility at this temperature restrict lateral grain coalescence and facet development, resulting in rounded grains with less distinct boundary definition. As the substrate temperature increases to 600 °C [Figures 4(c-d)], the grain size increases, indicating enhanced surface diffusion. Grain boundaries become sharper, and shallow faceting begins to emerge, consistent with a transition from nucleation-dominated growth to a competitive grain selection regime [18]. The film grown at 800 °C [Figures 4(e-f)] exhibits pronounced grain coarsening and faceted surface morphology,

This is the author's peer reviewed, accepted manuscript. However, the online version of record will be different from this version once it has been copyedited and typeset.

PLEASE CITE THIS ARTICLE AS DOI: 10.1063/1.50333162

with an average grain size of 192.5 nm and an RMS roughness of 25.7 nm. The increase in growth rate and surface mobility promotes the expansion of energetically favorable crystallites, resulting in polygonal faceting and elevated topographical features. This trend mirrors the morphology and coarsening behavior observed in Figure 1. The higher roughness at this temperature reflects greater vertical height contrast between facets, a signature of later-stage competitive grain growth in hydrogen-rich diamond CVD systems [18, 51]. Across all temperatures, the films remain continuous and conformal without delamination.

Figure 5 presents the room-temperature Raman spectra and optical absorption data for diamond films grown at 480 °C, 600 °C, and 800 °C. In the Raman spectra [Figure 5(a)], each diamond-coated sample exhibits a distinct sp^3 -bonded diamond peak near 1332 cm^{-1} , confirming successful diamond phase formation at all temperatures. The sharpness of this peak increases with growth temperature. This progressive narrowing indicates enhanced crystalline quality, aligning with the grain growth and surface evolution trends observed in SEM and AFM analyses in Figure 4. Because the deposition temperature directly influences the growth rate, the films grown at 480 °C, 600 °C, and 800 °C reached different thicknesses (58 nm, 110 nm, and 886 nm, respectively). Therefore, the observed Raman evolution reflects changes in growth kinetics with temperature and the corresponding differences in film thickness. The appearance of $\beta\text{-Ga}_2\text{O}_3$ substrate phonon modes in all spectra confirms the transparency of the diamond layers and preservation of substrate crystallinity throughout the CVD process. Figure 5(b) shows the optical absorption spectra of the same films, with the inset presenting Tauc plots used to estimate the effective optical absorption edge [52]. A systematic shift of the absorption edge toward higher energies is observed, with extracted values of 3.89 eV (480 °C), 4.22 eV (600 °C), and 5.13 eV (800 °C). This shift correlates with the increase in grain size and sp^3 -phase purity, and is influenced by both temperature and film

This is the author's peer reviewed, accepted manuscript. However, the online version of record will be different from this version once it has been copyedited and typeset.

PLEASE CITE THIS ARTICLE AS DOI: 10.1063/1.50333162

thickness, consistent with reduced sp^2 -related states and progressive microstructural refinement [53].

Figure 6 shows the surface morphological and spectroscopic properties of the films as a function of growth rate, which increases with substrate temperature from 480 °C to 800 °C. It should be noted that the temperature-dependent trends discussed in Figures 4-6 are inherently coupled with variations in growth rate and resulting film thickness; therefore, the observed evolution reflects the combined influence of temperature, growth kinetics, and thickness, rather than an isolated temperature effect. In Figure 6(a), both average grain size and RMS surface roughness increase with increasing growth rate and thickness (from 58 nm to 886 nm). These trends are consistent with a thermally activated transition from compact nanocrystallites at lower temperatures to larger, faceted grains at higher temperatures and greater deposition thickness. The observed morphological evolution is attributed to enhanced surface diffusion and increased adatom mobility, which promote lateral grain competition and selective expansion of energetically favorable crystallites [18,51]. Figure 6(b) shows the corresponding evolution of sp^3 -phase purity and Raman FWHM. As the growth rate increases from 29.1 nm/hr at 480 °C (58 nm thickness) to 354.4 nm/hr at 800 °C (886 nm thickness), the Raman FWHM narrows from 92.2 cm^{-1} to 51.34 cm^{-1} , consistent with improved structural coherence in larger grains [46]. In parallel, the sp^3 -phase purity increases from 96.1% at 58 nm to 98.9% at 886 nm, reflecting progressive suppression of sp^2 -bonded carbon during continued growth [18,50]. To evaluate the influence of dielectric interlayers under identical growth conditions, additional comparative Raman, SEM, and optical absorption analyses were performed for diamond films grown on 50 nm SiO_2 - and SiN_x -coated β - Ga_2O_3 substrates. The SiO_2 sample exhibited an average grain size of 126.6 nm and an sp^3 -phase purity of 97.1%, whereas the SiN_x sample showed a grain size of 106.5 nm and a phase purity of

This is the author's peer reviewed, accepted manuscript. However, the online version of record will be different from this version once it has been copyedited and typeset.

PLEASE CITE THIS ARTICLE AS DOI: 10.1063/5.0333162

96.9%. The extracted effective optical absorption edges were 5.13 eV and 5.11 eV, respectively. These small differences indicate only marginal interlayer influence under identical growth conditions. The complete datasets and detailed discussion are provided in the Supplementary Material (Fig. S3).

Figure 7 provides a comparative benchmarking analysis of sp^3 -phase purity as a function of diamond film thickness, incorporating representative literature reports of polycrystalline diamond films grown on foreign substrates [17-19, 38, 41, 54-61]. A general trend is observed across prior studies in which thinner films exhibit lower apparent sp^3 fractions, while continued growth and increased thickness correspond to progressive suppression of sp^2 -bonded carbon. The present work follows this established behavior, with sp^3 -phase purity increasing systematically from ~96% in ultrathin films to values approaching 99% for the 886 nm thick film. Notably, the high-purity data point achieved in this study lies within the upper range of reported values for hetero-integrated diamond films under comparable growth conditions.

In summary, this work presents a comprehensive investigation into the MPCVD growth of diamond films on β - Ga_2O_3 , demonstrating how processing conditions and interface engineering influence grain development, surface characteristics, and optical response. Thickness-dependent studies reveal a steady progression from densely nucleated nanocrystalline films to well-faceted surfaces, accompanied by lateral grain expansion and improved ordering during extended growth at a fixed temperature. As substrate temperature increases, enhanced surface mobility promotes grain coarsening and phase refinement, accompanied by higher growth rates and the resulting increase in film thickness. Notably, continuous, and phase-pure diamond films are achievable even at low temperature (480°C), highlighting the compatibility of this approach with device processing schemes constrained by limited thermal budgets.

This is the author's peer reviewed, accepted manuscript. However, the online version of record will be different from this version once it has been copyedited and typeset.

PLEASE CITE THIS ARTICLE AS DOI: 10.1063/1.50333162

See the Supplementary Material for additional experimental data and analysis supporting the main results. This includes control growth studies of diamond films on sapphire and Si substrates, comparative structural and optical characterization, and a detailed evaluation of the influence of SiO₂ and SiN_x dielectric interlayers on diamond growth on β-Ga₂O₃. Control experiments on sapphire show grain size increasing from ~50 nm to ~202 nm with thickness (58 to 824 nm), accompanied by an improvement in sp³-phase purity from ~97.3% to ~98.5%. Similarly, diamond films grown on Si exhibit large grain sizes (~246 nm) and high sp³-phase purity (~98.9%) at ~814 nm thickness, confirming dense, well-coalesced films. For β-Ga₂O₃ substrates, diamond films grown on SiO₂ and SiN_x interlayers under identical conditions exhibit comparable grain sizes (~126.6 nm vs. ~106.5 nm) and phase purity (~97.1% vs. ~96.9%), indicating only marginal influence of interlayer type.

Acknowledgement

The authors acknowledge the funding support from the National Science Foundation (NSF) under award numbers ECCS 2532898 and ECCS 2501623 and from the Air Force Research Laboratory Regional Network- Mid-Atlantic Hub.

Data Availability

The data that support the findings of this study are available from the corresponding author upon reasonable request.

Conflict of Interest

The authors have no conflicts to disclose.

References

This is the author's peer reviewed, accepted manuscript. However, the online version of record will be different from this version once it has been copyedited and typeset.

PLEASE CITE THIS ARTICLE AS DOI: 10.1063/5.0333162

- [1] A.J. Green, J. Speck, G. Xing, P. Moens, F. Allerstam, K. Gumaelius, T. Neyer, A. Arias-Purdue, V. Mehrotra, A. Kuramata, K. Sasaki, S. Watanabe, K. Koshi, J. Blevins, O. Bierwagen, S. Krishnamoorthy, K. Leedy, A.R. Arehart, A.T. Neal, S. Mou, S.A. Ringel, A. Kumar, A. Sharma, K. Ghosh, U. Singiseti, W. Li, K. Chabak, K. Liddy, A. Islam, S. Rajan, S. Graham, S. Choi, Z. Cheng, and M. Higashiwaki, *APL Mater.* **10**, 029201 (2022).
- [2] M. Higashiwaki, K. Sasaki, A. Kuramata, T. Masui, and S. Yamakoshi, *Appl. Phys. Lett.* **100**, 013504 (2012).
- [3] D. Wakimoto, C.-H. Lin, K. Ema, Y. Ueda, H. Miyamoto, K. Sasaki and A. Kuramata, *Appl. Phys. Express* **18**, 106502 (2025).
- [4] S.J. Pearton, F. Ren, M. Tadjer, and J. Kim, *J. Appl. Phys.* **124**, 220901 (2018).
- [5] Z. Guo, A. Verma, X. Wu, F. Sun, A. Hickman, T. Masui, A. Kuramata, M. Higashiwaki, D. Jena, and T. Luo, *Appl. Phys. Lett.* **106**, 111909 (2015).
- [6] J. Zhou, L. Zhong, X. Feng, W. Zhang, X. Liu, H. Zhou, Z. Liu, Y. Hao, and J. Zhang, *IEEE Trans. Electron Devices* **72**, 2769 (2025).
- [7] Z. Cheng, V. D. Wheeler, T. Bai; J. Shi, M. J. Tadjer; T. Feygelson, K. D. Hobart, M. S. Goorsky, S. Graham, *Appl. Phys. Lett.* **116**, 062105 (2020).
- [8] Y. Yamamoto, T. Imai, K. Tanabe, T. Tsuno, Y. Kumazawa, and N. Fujimori, *Diamond Related Mater.* **6**, 1057 (1997).
- [9] A.V. Sukhadolau, E.V. Ivakin, V.G. Ralchenko, A.V. Khomich, A.V. Vlasov, and A.F. Popovich, *Diamond Related Mater.* **14**, 589 (2005).
- [10] H.-Y. Cheng, C.-Y. Yang, L.-C. Yang, K.-C. Peng, C.-T. Chia, S.-J. Liu, I.-N. Lin, and K.-H. Lin, *J. Appl. Phys.* **123**, 165105 (2018).
- [11] J.E. Field, *Reports on Progress in Physics* **75**, 126505 (2012).
- [12] M. Higashiwaki, R. Kaplar, J. Pernot, and H. Zhao, *Appl. Phys. Lett.* **118**, 200401 (2021).
- [13] Y. Qin, B. Albano, J. Spencer, J.S. Lundh, B. Wang, C. Buttay, M. Tadjer, C. DiMarino, and Y. Zhang, *J. Phys. D: Appl. Phys.* **56**, 093001 (2023).
- [14] R. Kalish, *J. Phys. D: Appl. Phys.* **40**, 6467 (2007).
- [15] M. Malakoutian, R. Soman, K. Woo, and S. Chowdhury, *MRS Adv.* **9**, 7 (2023).
- [16] M. Malakoutian, X. Zheng, K. Woo, R. Soman, A. Kasperovich, J. Pomeroy, M. Kuball, and S. Chowdhury, *Adv. Func. Mater.* **32**, 2208997 (2022).
- [17] Y.S. Zou, Y. Yang, Y.M. Chong, Q. Ye, B. He, Z.Q. Yao, W.J. Zhang, S.T. Lee, Y. Cai, and H.S. Chu, *Cryst. Growth Des.* **8**, 1770 (2008).
- [18] M. Malakoutian, M.A. Laurent, and S. Chowdhury, *Crystals* **9**, 498 (2019).
- [19] M. Malakoutian, C. Ren, K. Woo, H. Li, and S. Chowdhury, *Cryst. Growth Des.* **21**, 2624 (2021).
- [20] S. Mandal, E.L. Thomas, C. Middleton, L. Gines, J.T. Griffiths, M.J. Kappers, R.A. Oliver, D.J. Wallis, L.E. Goff, S.A. Lynch, M. Kuball, and O.A. Williams, *ACS Omega* **2**, 7275 (2017).
- [21] M.A. Laurent, M. Malakoutian, and S. Chowdhury, *Semicond. Sci. Technol.* **35**, 015003 (2020).
- [22] M. Malakoutian, A. Kasperovich, D. Rich, K. Woo, C. Perez, R. Soman, D. Saraswat, J. Kim, M. Noshin, M. Chen, S. Vaziri, X. Bao, C.C. Shih, W.-Y. Woon, M. Asheghi, K.E. Goodson, S.S. Liao, S. Mitra, and S. Chowdhury, *Cell Rep. Phys. Sci.* **4**, 101686 (2023).
- [23] O.A. Williams, S. Mandal, and J.A. Cuenca, *Acc. Mater. Res.* **5**, 1172 (2024).
- [24] B.V. Spitsyn, L.L. Bouilov, and B.V. Derjaguin, *J. Cryst. Growth* **52**, 219 (1981).
- [25] N. Fujimori, T. Imai, and A. Doi, *Vacuum* **36**, 99 (1986).

This is the author's peer reviewed, accepted manuscript. However, the online version of record will be different from this version once it has been copyedited and typeset.

PLEASE CITE THIS ARTICLE AS DOI: 10.1063/5.0333162

- [26] S. Yugo, T. Kimura, H. Kanai, and Y. Adachi, *MRS Proc.* **97**, 327 (1987).
- [27] C.-P. Chang, D.L. Flamm, D.E. Ibbotson, and J.A. Mucha, *J. Appl. Phys.* **63**, 1744 (1988).
- [28] S. Yugo, T. Kanai, T. Kimura, and T. Muto, *Appl. Phys. Lett.* **58**, 1036 (1991).
- [29] S. Yugo, T. Kanai, and T. Kimura, *Diamond Related Mater.* **1**, 388 (1992).
- [30] K. Tsugawa, M. Ishihara, J. Kim, Y. Koga, and M. Hasegawa, *J. Phys. Chem. C* **114**, 3822 (2010).
- [31] R.N. Tiwari and L. Chang, *J. Appl. Phys.* **107**, 103305 (2010).
- [32] R.N. Tiwari, J.N. Tiwari, and L. Chang, *Chem. Eng. J.* **158**, 641 (2010).
- [33] R.N. Tiwari and L. Chang, *Appl. Phys. Exp.* **3**, 045501 (2010).
- [34] P.A. Bianconi, S.J. Joray, B.L. Aldrich, J. Sumranjit, D.J. Duffy, D.P. Long, J.L. Lazorcik, L. Raboin, J.K. Kearns, S.L. Smulligan, and J.M. Babyak, *J. Am. Chem. Soc.* **126**, 3191 (2004).
- [35] Y. Nur, H.M. Cengiz, M.W. Pitcher, and L.K. Toppare, *J. Mat. Sci.* **44**, 2774 (2009).
- [36] V.S. Sedov, V.G. Ralchenko, T.M. Zvukova, and A.I. Sizov, *Diamond Related Mater.* **74**, 65 (2017).
- [37] S. Mandal, *RSC Adv.* **11**, 10159 (2021).
- [38] A.V. Sumant, P.U.P.A. Gilbert, D.S. Grierson, A.R. Konicek, M. Abrecht, J.E. Butler, T. Feygelson, S.S. Rotter, and R.W. Carpick, *Diamond Related Mater.* **16**, 718 (2007).
- [39] S. Mandal, K. Arts, H.C.M. Knoops, J.A. Cuenca, G.M. Klemencic, and O.A. Williams, *Carbon* **181**, 79 (2021).
- [40] W.D. Harkins, *J. Chem. Phys.* **10**, 268 (1942).
- [41] I. Rahaman, M. Sultana, R. Medina, I. Emu, and A. Haque, *Mat. Sci. Semicond. Proc.* **184**, 108808 (2024).
- [42] M. Malakoutian, Y. Song, C. Yuan, C. Ren, J.S. Lundh, R.M. Lavelle, J.E. Brown, D.W. Snyder, S. Graham, S. Choi, and S. Chowdhury, *Appl. Phys. Exp.* **14**, 055502 (2021).
- [43] H.N. Masten, J.S. Lundh, T.I. Feygelson, K. Sasaki, Z. Cheng, J.A. Spencer, P.-Y. Liao, J.K. Hite, D.J. Pennachio, A.G. Jacobs, M.A. Mastro, B.N. Feigelson, A. Kuramata, P. Ye, S. Graham, B.B. Pate, K.D. Hobart, T.J. Anderson, and M.J. Tadjer, *Appl. Phys. Lett.* **124**, 153502 (2024).
- [44] H.A. Girard, S. Perruchas, C. Gesset, M. Chaigneau, L. Vieille, J.-C. Arnault, P. Bergonzo, J.-P. Boilot, and T. Gacoin, *ACS Appl. Mater. Interfaces* **1**, 2738 (2009).
- [45] R. Rajasekar, N.H. Kim, D. Jung, T. Kuila, J.K. Lim, M.J. Park, and J.H. Lee, *Composites Science and Technology* **89**, 167 (2013).
- [46] S. Osswald, V.N. Mochalin, M. Havel, G. Yushin, and Y. Gogotsi, *Physical Review B* **80**, 075419 (2009).
- [47] R. Tu, T. Xu, D. Li, S. Zhang, M. Yang, Q. Li, L. Zhang, T. Shimada, T. Goto, and J. Shi, *RSC Adv.* **8**, 16061 (2018).
- [48] N. Wada and S. A. Solin, *Phys. B+C* **105**, 353 (1981).
- [49] R. E. Shroder, R. J. Nemanich, and J. T. Glass, *Phys. Rev. B* **41**, 3738–3745 (1990).
- [50] M. Eckert, E. Neyts, and A. Bogaerts, *Cryst. Growth Des.* **10**, 3005 (2010).
- [51] J.E. Butler and A.V. Sumant, *Chemical Vapor Deposition* **14**, 145 (2008).
- [52] P. Makula, M. Pacia, and W. Macyk, *The Journal of Physical Chemistry Letters* **9**, 6814 (2018).
- [53] C. Wang, D. Shinyavskiy, L. Suter, Z. Altikriti, Q. Jia, M. Muehle, and J. Seo, *Advanced Science* **12**, e03986 (2025).

This is the author's peer reviewed, accepted manuscript. However, the online version of record will be different from this version once it has been copyedited and typeset.

PLEASE CITE THIS ARTICLE AS DOI: 10.1063/5.0333162

- [54] D.M. Gruen, A.R. Krauss, C.D. Zuiker, R. Csencsits, L.J. Terminello, J.A. Carlisle, I. Jimenez, D.G. Sutherland, D.K. Shuh, W. Tong, and F.J. Himpsel, *Appl. Phys. Lett.* **68**, 1640 (1996).
- [55] J. Liu, L. Hei, G. Chen, C. Li, W. Tang, and F. Lu, *Carbon* **60**, 564 (2013).
- [56] A.V. Sumant, O. Auciello, H.-C. Yuan, Z. Ma, R.W. Carpick, and D.C. Mancini, *Proc. of SPIE* **7318**, 731817 (2009).
- [57] A. Tallaire, C. Rond, F. Bénédic, O. Brinza, J. Achard, F. Silva, and A. Gicquel, *Phys. Stat. Sol. A* **208**, 2028 (2011).
- [58] J.V. Silva Neto, J.S. Gómez, E.J. Corat, and V.J. Trava-Airoldi, *Mater. Res.* **25**, e20220052 (2022).
- [59] T. Guillemet, Z.Q. Xie, Y.S. Zhou, J.B. Park, A. Veillere, W. Xiong, J.M. Heintz, J.F. Silvain, N. Chandra, and Y.F. Lu, *ACS Appl. Mater. Interfaces* **3**, 4120 (2011).
- [60] A. Dychalska, P. Popielarski, W. Franków, K. Fabisiak, K. Paprocki, and M. Szybowicz, *Mat. Sci. Poland* **33**, 799 (2015).
- [61] A. Haque, S. Gupta, and J. Narayan, *ACS Appl. Electron Mater.* **2**, 1323 (2020).

This is the author's peer reviewed, accepted manuscript. However, the online version of record will be different from this version once it has been copyedited and typeset.

PLEASE CITE THIS ARTICLE AS DOI: 10.1063/1.50333162

Figure 1

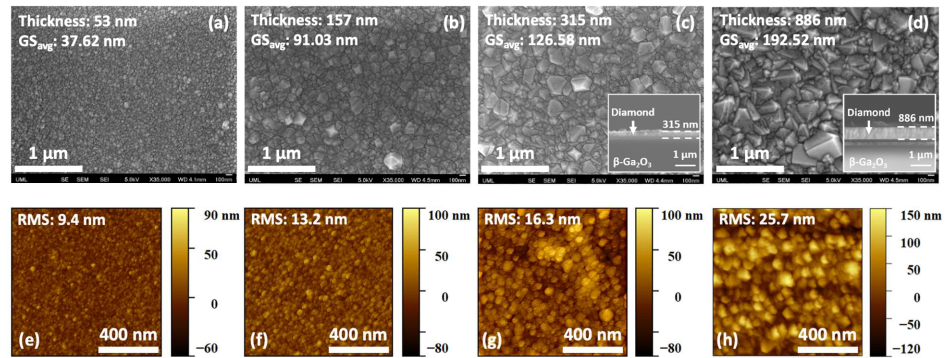


Figure 1. Surface morphology and roughness evolution of diamond films grown at 800 °C for 10, 30, 60 and 150 minutes: (a-c) SEM images and (d-f) corresponding AFM scans showing increasing grain size, faceting and RMS roughness.

This is the author's peer reviewed, accepted manuscript. However, the online version of record will be different from this version once it has been copyedited and typeset.

PLEASE CITE THIS ARTICLE AS DOI: 10.1063/1.50333162

Figure 2

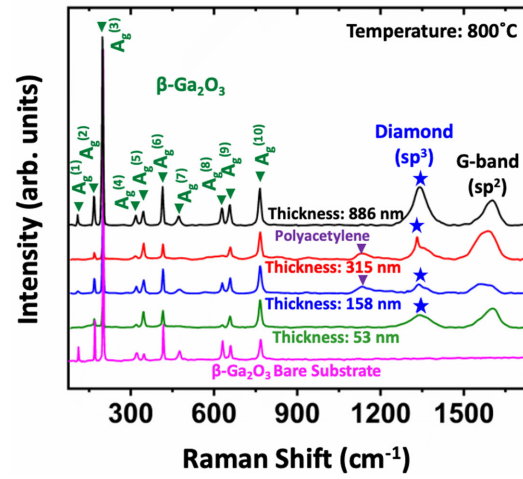


Figure 2. Raman spectra of diamond films grown at 800 °C, showing intensification of the sp³ diamond peak with increasing film thickness.

This is the author's peer reviewed, accepted manuscript. However, the online version of record will be different from this version once it has been copyedited and typeset.
 PLEASE CITE THIS ARTICLE AS DOI: 10.1063/1.50333162

Figure 3

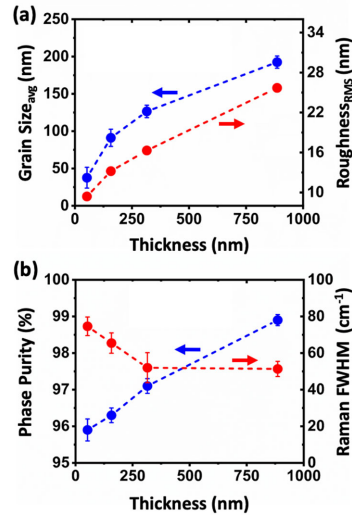


Figure 3. Grain size, surface roughness, Raman FWHM, and sp³-phase purity as a function of diamond film thickness grown at 800 °C.

This is the author's peer reviewed, accepted manuscript. However, the online version of record will be different from this version once it has been copyedited and typeset.
 PLEASE CITE THIS ARTICLE AS DOI: 10.1063/1.50333162

Figure 4

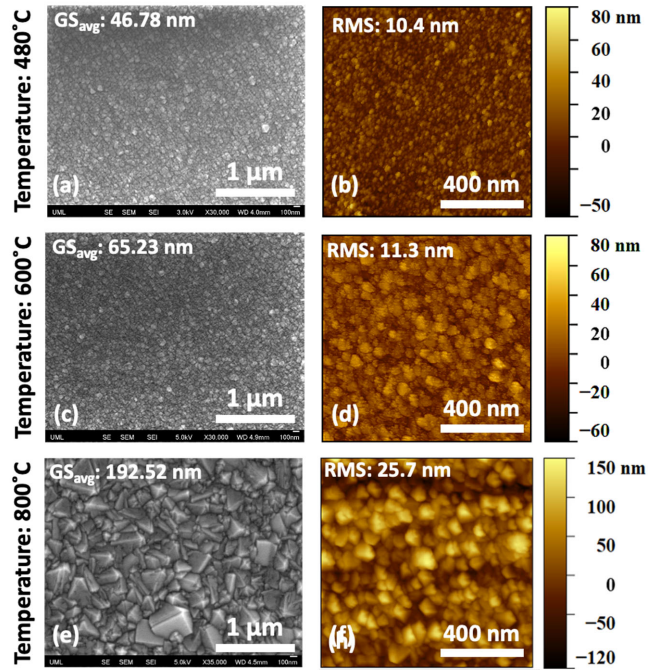


Figure 4. (a,c,e) SEM and (b,d,f) AFM images showing temperature-dependent evolution of surface morphology, grain size, and roughness of diamond films grown at 480 °C, 600 °C, and 800 °C.

This is the author's peer reviewed, accepted manuscript. However, the online version of record will be different from this version once it has been copyedited and typeset.

PLEASE CITE THIS ARTICLE AS DOI: 10.1063/1.50333162

Figure 5

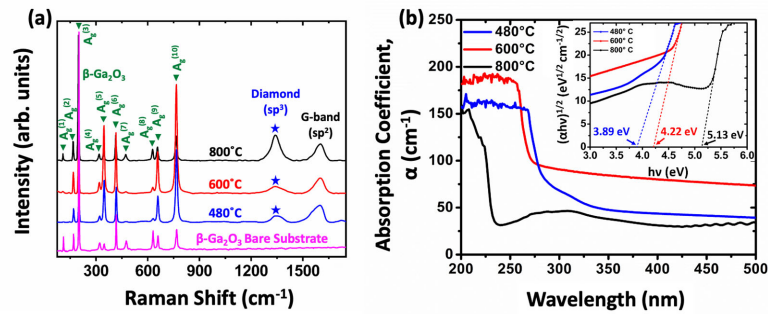


Figure 5. (a) Raman and (b) optical absorption spectra of diamond films grown at 480 °C, 600 °C, and 800 °C.

This is the author's peer reviewed, accepted manuscript. However, the online version of record will be different from this version once it has been copyedited and typeset.
 PLEASE CITE THIS ARTICLE AS DOI: 10.1063/1.50333162

Figure 6

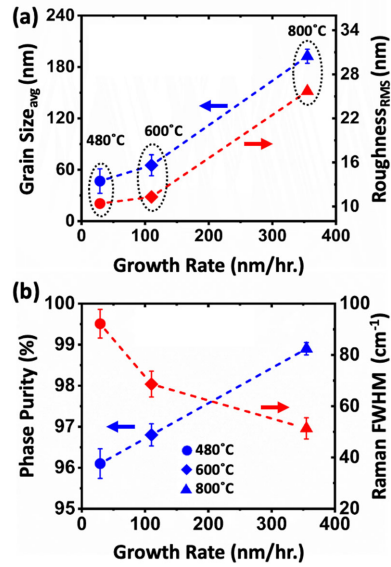


Figure 6. (a) Average grain size and surface roughness, and (b) Raman FWHM and sp^3 -phase purity of diamond films as a function of growth rate achieved at substrate temperatures of 480 °C, 600 °C, and 800 °C.

This is the author's peer reviewed, accepted manuscript. However, the online version of record will be different from this version once it has been copyedited and typeset.

PLEASE CITE THIS ARTICLE AS DOI: 10.1063/1.50333162

Figure 7

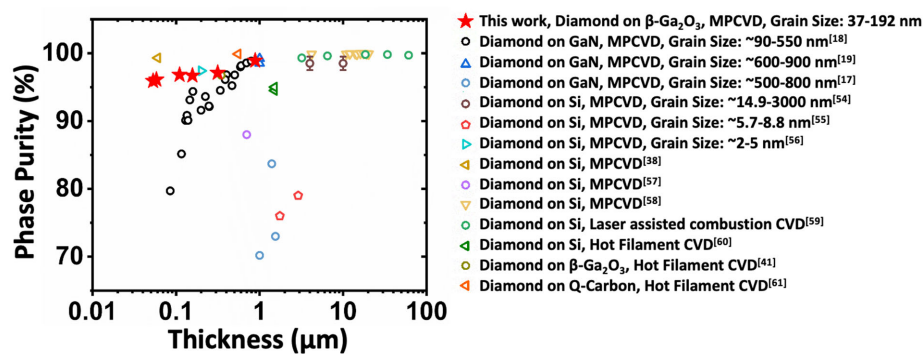


Figure 7. Benchmark comparison of sp³-phase purity as a function of diamond film thickness for the present work and representative literature reports of polycrystalline diamond grown on foreign substrates using various CVD techniques.

Supplementary Material

Microwave plasma CVD growth and characterization of polycrystalline diamond films on β -Ga₂O₃

Saleh Ahmed Khan¹, Stephen Margiotta¹, Ahmed Ibreljic¹, Anhar Bhuiyan^{1, a)}

¹*Department of Electrical and Computer Engineering, University of Massachusetts Lowell, MA 01854, USA*

^{a)} Corresponding author Email: anhar_bhuiyan@uml.edu

I. Diamond Growth on Sapphire Substrates:

Control growth experiments were performed on c-plane sapphire substrates under MPCVD conditions comparable to those used for β -Ga₂O₃ (50 Torr, 1% CH₄/H₂, polymer-assisted nanodiamond seeding). Raman spectra [Supplementary Fig. S1(a)] confirm the formation of diamond with characteristic sp³ features near 1332 cm⁻¹. Two films with thicknesses of approximately 58 nm and 824 nm were grown under these conditions. The 58 nm film exhibits an average grain size of ~50 nm and an sp³-phase purity of ~97.3%, whereas the 824 nm film shows substantially larger grains (~202 nm) and an improved phase purity of ~98.5%. Cross-sectional imaging verifies uniform film coverage and good adhesion to the sapphire surface. These observations are consistent with progressive microstructural refinement during continued MPCVD deposition and provide a useful cross-substrate reference, indicating that the sp³-phase fractions and grain coarsening behavior observed on β -Ga₂O₃ follow the same trend, where increased film thickness is associated with improved sp³-phase purity.

Table S1. Diamond films deposited on sapphire substrates.

Alt Text: Summary of diamond films grown on sapphire showing that increasing film thickness leads to larger grain size and higher sp³ phase purity, indicating improved crystallinity with continued growth.

Sample	Substrate	Diamond Thickness (nm)	Grain Size (nm)	Phase Purity (%)
1	SiO ₂ /Sapphire	824	202	98.5
2	SiO ₂ /Sapphire	58	50	97.3

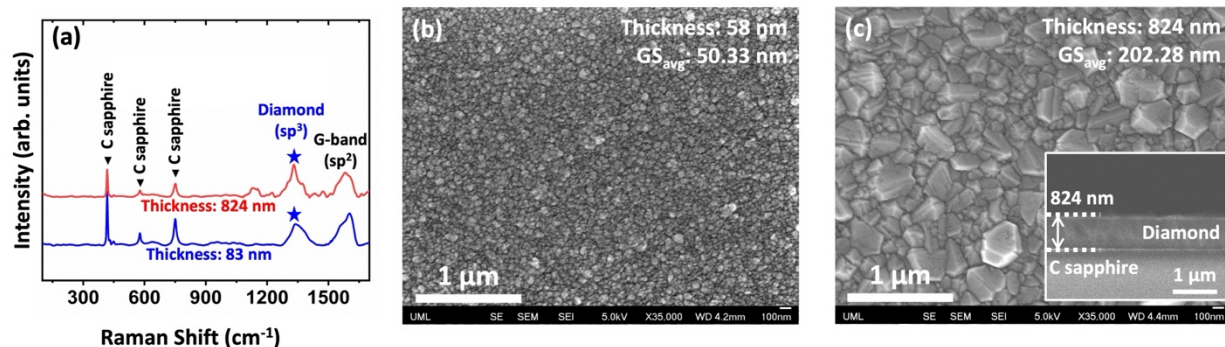


Figure S1. Diamond growth on sapphire substrates. (a) Room-temperature Raman spectra of diamond films grown on sapphire, showing the characteristic sp^3 diamond peak near 1332 cm^{-1} . (b) Top-view SEM image of a $\sim 58\text{ nm}$ thick film exhibiting fine-grained morphology ($GS_{\text{avg}} \approx 50\text{ nm}$). (c) Top-view and cross-sectional SEM images of a thicker ($\sim 824\text{ nm}$) film showing significant grain coarsening ($GS_{\text{avg}} \approx 202\text{ nm}$) and continuous film coverage on sapphire.

Alt Text: Diamond films grown on sapphire showing thickness-dependent grain growth. Grain size increases and crystallinity improves with increasing film thickness, consistent with progressive microstructural refinement during MPCVD growth.

II. Diamond Growth on Si Substrates:

Control diamond growth experiments were also carried out on Si substrates under comparable MPCVD and polymer-assisted nanodiamond seeding conditions (50 Torr, 1% CH_4/H_2) for a deposition duration of 150 minutes. The Raman spectrum [Supplementary Fig. S2(a)] exhibits a well-defined sp^3 diamond peak near 1332 cm^{-1} , corresponding to a sp^3 -phase purity of 98.9%. Top-view SEM imaging [Supplementary Fig. S2(b)] reveals a dense, faceted polycrystalline morphology with an average grain size of $\sim 246\text{ nm}$ following extended deposition. Cross-sectional SEM analysis [Supplementary Fig. S2(c)] confirms continuous film coverage with a thickness of $\sim 814\text{ nm}$ and uniform adhesion to the underlying silicon substrate.

Table S2. Diamond films deposited on Si substrates.

Alt Text: Summary of diamond films grown on Si substrates showing large grain size and high sp^3 phase purity after extended growth, consistent with dense and well-coalesced polycrystalline films.

Sample	Substrate	Diamond Thickness (nm)	Grain Size (nm)	Phase Purity (%)
1	Si	814	246	98.9

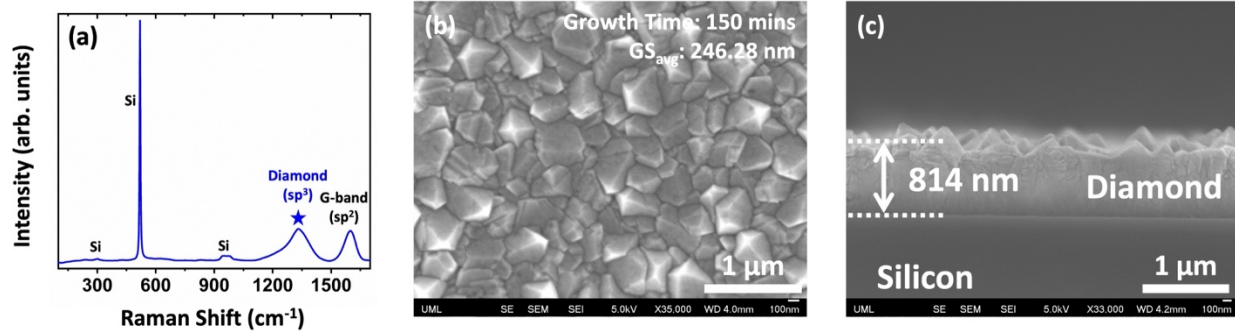


Figure S2. Diamond growth on Si substrates. (a) Room-temperature Raman spectrum showing a prominent sp^3 diamond peak near 1332 cm^{-1} . (b) Top-view SEM image of the $\sim 814\text{ nm}$ thick film grown for 150 minutes, exhibiting well-developed faceted grains ($GS_{\text{avg}} \approx 246\text{ nm}$). (c) Cross-sectional SEM image confirming uniform film thickness ($\sim 814\text{ nm}$) and continuous diamond coverage on the Si substrate.

Alt Text: Diamond films grown on Si substrate showing dense and continuous coverage. Large faceted grains and high sp^3 phase purity are observed, indicating effective coalescence and improved film quality.

III. Influence of Dielectric Interlayers on Diamond Growth on $\beta\text{-Ga}_2\text{O}_3$:

To assess the influence of dielectric interlayers on diamond film quality, Figure S3 compares the structural and optical properties of diamond films grown under identical MPCVD conditions on SiO_2 - and SiN_x -coated $\beta\text{-Ga}_2\text{O}_3$ substrates. Both interlayers were deposited to a thickness of 50 nm via PECVD at $300\text{ }^\circ\text{C}$ and 1 Torr using a plasma power of 20 W. The SiO_2 films were deposited using an $\text{N}_2\text{O}/\text{SiH}_4$ chemistry, yielding a refractive index of 1.47, consistent with near-stoichiometric oxide [1, 2]. SiN_x films were deposited using an $\text{N}_2/\text{NH}_3/\text{SiH}_4$ chemistry, resulting in a refractive index of 1.91. This value lies within the typical range reported for PECVD silicon nitride films ($n \approx 1.8 - 2.1$), where the refractive index depends strongly on deposition conditions and film composition, particularly the Si/N ratio [3-5]. PECVD SiN_x films deposited near $300\text{ }^\circ\text{C}$

are generally non-stoichiometric and contain bonded hydrogen (Si-H and N-H), with reported N/Si ratios of ~1.2 - 1.35 and hydrogen contents of ~10 - 30 at.% depending on growth conditions [3-5]. Diamond growth was then performed under identical MPCVD conditions, including a substrate temperature of 800 °C, pressure of 50 Torr, CH₄/H₂ ratio of 1%, and growth duration of 60 minutes. SEM micrographs reveal that the film grown on SiO₂ exhibits an average lateral grain size of 126.6 nm, while the SiN_x-buffered counterpart shows an average grain size of 106.5 nm. The modest difference in grain size suggests that the interlayer may exert a limited influence on surface energetics or early-stage nucleation dynamics, but the overall microstructural evolution remains comparable under the same growth conditions. In addition, the continuous and conformal surface morphology without observable discontinuities or delamination suggests robust film integrity; however, atomic-resolution interface-sensitive characterization (e.g., scanning transmission electron microscopy combined with electron energy loss spectroscopy (STEM-EELS)) is required for definitive assessment of interfacial structure, bonding, and chemical composition, including potential interfacial reactions or diffusion at the Ga₂O₃-interlayer-diamond interface. The corresponding phase purity, estimated from Raman analysis, is 97.1% for the SiO₂ sample and 96.9% for the SiN_x sample. The Raman spectra in Figure S3(a) for both samples exhibit diamond peaks near 1332 cm⁻¹ and similar secondary features attributed to polyacetylene and sp²-bonded carbon. While slight differences in FWHM are observed, both films demonstrate comparable crystalline quality and successful diamond phase formation. The presence of β-Ga₂O₃ substrate phonon modes in both spectra confirms the transparency of the diamond layers and preservation of substrate structural integrity during growth. Figure S3(b) shows the optical absorption spectra and extracted Tauc plots. The film on SiO₂ exhibits an effective optical absorption edge of 5.13 eV, while the SiN_x-based film shows a comparable value of 5.11 eV. The

small difference between these values falls within experimental uncertainty, indicating that the dielectric interlayer has only a marginal impact on the intrinsic optical transition. Although only marginal differences are observed between SiO₂ and SiN_x interlayers under identical growth conditions, subtle variations in surface chemistry and interfacial energetics may influence early-stage nucleation and subsequent microstructural evolution. Differences in surface hydroxylation, charge distribution, and electrostatic interaction with the polymer-assisted nanodiamond layer could affect initial seed attachment and local nucleation density [6-8]. Variations in surface energy between oxide and nitride layers [9, 10] may also influence island wetting behavior and grain expansion kinetics during continued growth. Under hydrogen-rich plasma conditions, both interlayers act as chemically stable diffusion barriers that mitigate direct plasma interaction with β -Ga₂O₃ [11, 12]. Further interfacial characterization would be required to quantify these effects definitively.

Table S3. Structural and optical properties of diamond films grown on 50 nm SiO₂- and SiN_x-coated β -Ga₂O₃ substrates under identical MPCVD conditions (800 °C, 50 Torr, CH₄/H₂ = 1%, 60 min).

Alt Text: Comparison of diamond films grown on SiO₂- and SiN_x-coated β -Ga₂O₃ under identical conditions.

Sample	Interlayer	Diamond Thickness (nm)	Grain Size (nm)	Phase Purity (%)
1	SiO ₂	315	126.6	97.1
2	SiN _x	315	106.5	96.9

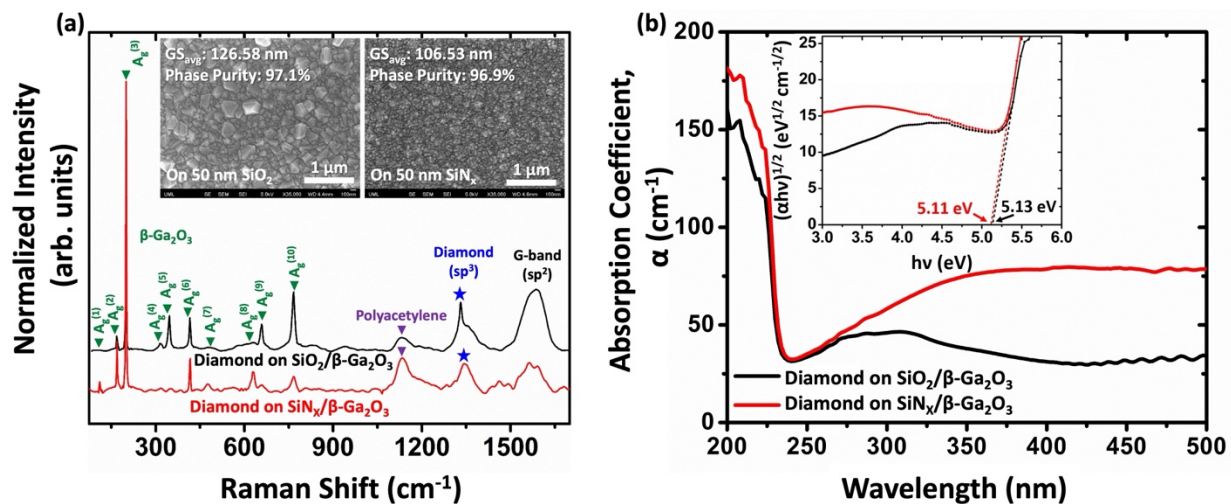


Figure S3. (a) Raman spectra and SEM images (insets) comparing grain size and phase purity of diamond films grown on SiO₂- and SiN_x-coated β-Ga₂O₃; (b) corresponding optical absorption spectra with extracted effective optical absorption edge.

Alt Text: Comparison of diamond films grown on SiO₂- and SiN_x-coated β-Ga₂O₃ under identical conditions.

References:

- [1] W. A. Pliskin and H. S. Lehman, *J. Electrochem. Soc.* 112, 1013 (1965)
- [2] P. N. K. Deenapanray, J. Lengyel, H. H. Tan, M. Petracic, A. Durandet, J. S. Williams, and C. Jagadish, *MRS Online Proceedings Library* 555, 197–202 (1998)
- [3] F. Karouta, K. Vora, J. Tian and C. Jagadish, *J. Phys. D: Appl. Phys.* 45, 445301 (2012)
- [4] W. A. P. Claassen, W. G. J. N. Valkenburg, F. H. P. M. Habraken, and Y. Tamminga, *J. Electrochem. Soc.* 130 2419–23 (1983)
- [5] W. A. Lanford; M. J. Rand, *J. Appl. Phys.* 49, 2473 (1978)
- [6] H.A. Girard, S. Perruchas, C. Gesset, M. Chaigneau, L. Vieille, J.-C. Arnault, P. Bergonzo, J.-P. Boilot, and T. Gacoin, *ACS Appl. Mater. Interfaces* 1, 2738 (2009).
- [7] P.A. Bianconi, S.J. Joray, B.L. Aldrich, J. Sumranjit, D.J. Duffy, D.P. Long, J.L. Lazorcik, L. Raboin, J.K. Kearns, S.L. Smulligan, and J.M. Babyak, *J. Am. Chem. Soc.* 126, 3191 (2004).
- [8] S. Mandal, *RSC Adv.* 11, 10159 (2021).
- [9] S. Mandal, K. Arts, H.C.M. Knoop, J.A. Cuenca, G.M. Klemencic, and O.A. Williams, *Carbon* 181, 79 (2021).
- [10] M. Malakoutian, M.A. Laurent, and S. Chowdhury, *Crystals* 9, 498 (2019).
- [11] J.E. Butler and A.V. Sumant, *Chemical Vapor Deposition* 14, 145 (2008).
- [12] M. Malakoutian, Y. Song, C. Yuan, C. Ren, J.S. Lundh, R.M. Lavelle, J.E. Brown, D.W. Snyder, S. Graham, S. Choi, and S. Chowdhury, *Appl. Phys. Exp.* 14, 055502 (2021).